Hindawi Publishing Corporation
Journal of Nanomaterials
Volume 2014, Article ID 138561, 7 pages
http://dx.doi.org/10.1155/2014/138561

Research Article

Hydrothermal Synthesis, Characterization, and Visible Light-Driven Photocatalytic Properties of Bi_2WO_6 Nanoplates

Anukorn Phuruangrat,[1] Phattranit Dumrongrojthanath,[2] Nuengruethai Ekthammathat,[2] Somchai Thongtem,[3,4] and Titipun Thongtem[2,4]

[1] *Department of Materials Science and Technology, Faculty of Science, Prince of Songkla University, Hat Yai, Songkhla 90112, Thailand*
[2] *Department of Chemistry, Faculty of Science, Chiang Mai University, Chiang Mai 50200, Thailand*
[3] *Department of Physics and Materials Science, Faculty of Science, Chiang Mai University, Chiang Mai 50200, Thailand*
[4] *Materials Science Research Center, Faculty of Science, Chiang Mai University, Chiang Mai 50200, Thailand*

Correspondence should be addressed to Anukorn Phuruangrat; phuruangrat@hotmail.com
and Titipun Thongtem; ttpthongtem@yahoo.com

Received 8 January 2014; Revised 9 April 2014; Accepted 9 April 2014; Published 7 May 2014

Academic Editor: Tao He

In this research, the effects on reaction temperature and length of time on Bi_2WO_6 nanoplates by hydrothermal synthesis on morphologies and photocatalytic properties were studied. The products obtained at different reaction temperature and reaction time were characterized by XRD, Raman, FTIR, SEM, and TEM techniques. The photocatalytic properties of the samples were measured by decomposing the rhodamine-B organic dye. XRD pattern was specified as pure orthorhombic well-crystallized Bi_2WO_6 phase for the 180°C and 20 h synthesis. Its FTIR spectrum shows main absorption bands at 400–1000 cm^{-1}, assigned to Bi–O stretching, W–O stretching, and W–O–W bridging stretching modes. SEM and TEM analyses show that the product was composed of nanoplates. Photocatalytic activity of Bi_2WO_6 nanoplates shows the 98.24% degradation of rhodamine-B under the Xe light irradiation within 100 min.

1. Introduction

In the past three decades, semiconducting photocatalyst has attracted extensive attention due to its potential applications in solar energy conversion and environmental remedy [1, 2]. Because of the good chemical stability, high oxidation activity, nontoxicity, and low price, TiO_2 has been the most popular photocatalyst for environmental purification. Among different semiconductors, titania has been investigated most frequently since the discovery of the photocatalytic splitting of water on titania electrodes in 1972 by Fujishima and Honda [1, 3, 4]. The main shortcoming of titania is the absorption of only ultraviolet with the wavelength of less than 387.5 nm, which accounts for only about 4% of sunlight. TiO_2-based photocatalysts have been the most popular and have been shown to be a lot of progress. Due to the fact that TiO_2 can only be activated by the ultraviolet light, the use of TiO_2 is thus limited by its negligible activity under visible light irradiation [4, 5]. It is very urgent to develop highly efficient visible light induced photocatalysts to meet the high requirement of future environmental remedy and energy crisis. Therefore, it is of great importance to develop visible light responsive photocatalysts.

Bismuth tungstate was reported to show photocatalytic activity under visible light irradiation [1, 5]. The Aurivillius family of bismuth oxide layered perovskite has attracted considerable attention due to their important applied properties such as ionic conductivity, photocatalytic activity in waste purification, and ferroelectricity [6, 7]. Their common formula $[Bi_2O_2][A_{n-1}B_nO_{3n+1}]$ (A = Ca, Sr, Ba, Pb, Bi, Na, K, and B = Ti, Nb, Ta, Mo, W, Fe) suggests easy tuning of these properties by iso- or aliovalent substitution at the A and B perovskitic sites with an only empirical restriction that the B position should be occupied with ions with the

radius of ca. 0.6 Å and over 60% of them having nd^0 electron configuration. The $n = 1$ case differs significantly from $n > 1$ series in several aspects. First, there are no A positions in the perovskitic slabs, and the possibilities of isovalent substitution among ferroelectrics are very restricted [4–6]. Bi_2WO_6 as an Aurivillius-phase perovskite belongs to the bismuth oxide family with a structure consisting of perovskite layers ($A_{m-1}B_mO_{3m+1}$) between corner-sharing structure of WO_6 octahedrons sandwiched between $(Bi_2O_2)^{2+}$ layers [8–10]. Bismuth tungstate (Bi_2WO_6) is a typical n-type direct band gap semiconductor with a band gap of 2.75 eV and has potential applications in electrode materials, solar energy conversion, and visible-light-driven photocatalysis [9].

The Bi_2WO_6 nanostructures with different morphologies such as nanoplates [4, 11], nanocages [7], hierarchical flowers [8], snow-like [9], and nanolaminars [10] have been prepared by solution-phase methods such as hydrothermal [4, 8, 9, 11], refluxing [7], sonochemical method [10], and citrate complex method [12]. However, the hydrothermal method is a widely used technique because of low cost, low temperature, high yield, scalable process, and large scale method [13, 14]. It is able to control the shape and dimension of nanomaterials by reaction time, temperature, pH value, and capping agent during hydrothermal process [13, 15, 16]. Shang et al. [4] prepared Bi_2WO_6 photocatalytic nanoplates with the size of ca. 30 nm. The photocatalytic activity of the as-prepared Bi_2WO_6 was evaluated by the degradation of rhodamine-B (RhB) solution under visible light irradiation within 60 min while photodegradation efficiency of RhB of Bi_2WO_6 nanoparticles reaches 75 min [17]. It was about 8–10 times higher than that of the product prepared by solid-state reaction.

In the present study, we report a facile, low-cost, and green hydrothermal route to synthesize the Bi_2WO_6 nanoplates. The effects of hydrothermal temperature and reaction time on formation of Bi_2WO_6 nanoplates, as well as their photocatalytic activities, were investigated. It was found that the Bi_2WO_6 nanoplates have high visible light photocatalytic activity in the degradation of RhB.

2. Experimental Procedures

Several solutions were formed by dissolving 1.6493 g of sodium tungstate (Na_2WO_4) in 100 mL reverse osmosis (RO) water each and continuously stirred at room temperature for 30 min. Subsequently, 4.8511 g bismuth nitrate ($Bi(NO_3)_3$) was added to each of these solutions with 30 min continuous stirring at room temperature and followed by adding 3 M NaOH until achieving the desired pH of 10. The solutions were hydrothermally processed at 100–200°C for 0–20 h. In the end, the as-synthesized precipitates were separated by filtration, rinsed with distilled water and ethanol, and dried at 80°C for 24 h for further characterization.

X-ray powder diffraction (XRD) patterns of the products were recorded on a Japan Rigaku D/MAX-γA X-ray diffractometer with graphite monochromator and Cu K_α radiation (λ = 0.154178 nm) at a scanning rate of 0.02 deg/s ranging from 20 to 60 deg. Raman spectra were recorded on a HORIBA JOBIN YVON T64000 Raman spectrometer with 50 mW and 514.5 nm wavelength Ar green laser and FTIR spectra on a BRUKER TENSOR 27 Fourier transform infrared (FTIR) spectrometer with KBr as a diluting agent and operated in the range of 400–4,000 cm^{-1}. SEM images were taken on a JEOL JSM-6335F scanning electron microscope operating at 20 kV and TEM images on a JEOL JEM-2010 JEOL transmission electron microscope (TEM) at an accelerating voltage of 200 kV. UV-visible absorption was carried out on a Perkin Elmer Lambda 25 UV-vis spectrophotometer.

The photocatalytic activities of as-synthesized samples were tested by measuring the degradation of rhodamine-B (RhB) in an aqueous solution under visible light irradiation as light source of Xe lamp. Each 150 mg photocatalyst was suspended in each of 150 mL 10^{-5} M RhB solution aqueous solutions. The solutions were magnetically stirred for 30 min in dark to establish an adsorption/desorption equilibrium of RhB on the surfaces of the photocatalyst. Then the light was turned on to initiate the photocatalytic reaction. The solution was analyzed by a Lambda 25 spectrophotometer, using 450 W of Xe lamp with wavelength of 553 nm. The decolorization efficiency (%) has been calculated as follows:

$$\text{Decolorization efficiency } (\%) = \frac{C_o - C}{C_o} \times 100, \quad (1)$$

where C_o is the initial concentration of RhB and C is the concentration of RhB after light irradiation.

3. Results and Discussion

To investigate the formation process of Bi_2WO_6 phase, XRD patterns of the samples processed at different temperatures and lengths of time were characterized and shown in Figure 1. The temperature and time have a great influence on the formation of the crystals. Figure 1(a) shows the XRD patterns of the as-synthesized samples at 100–200°C for 20 h by hydrothermal method. It was clearly seen that the crystallization has occurred even at 100°C which can be indexed to Bi_2WO_6 mixed with cubic Bi_2O_3 phase according to the JCPDS number 27-0052 [18]. When the temperature further goes up to 200°C, the XRD patterns of the sample reveal the narrower peaks and the higher intensity, suggesting the enhanced crystallite size. However, the intensities of all diffraction peaks of Bi_2WO_6 synthesized at 180°C for 20 h are the same as the Bi_2WO_6 at 200°C for 20 h. Therefore, the hydrothermally temperature of 180°C is high enough for synthesizing of Bi_2WO_6. At 180 and 200°C, all the diffraction peaks can be readily indexed as pure orthorhombic well-crystallized Bi_2WO_6 structure with cell parameters of a = 5.46 Å, b = 5.44 Å, and c = 16.43 Å, in good agreement with those of the JCPDS number 73-1126 [18]. It was found that the standard intensity of the (113) peak is about five times higher than that of the (200) peak which could be expressed as $I_{(113)}/I_{(200)} = 5$. However, as for the sample prepared at 180°C for 20 h, the value of $I_{(113)}/I_{(200)}$ was 2.63, suggesting that the crystal has special anisotropic growth in (200) direction [11]. Therefore, the temperature reaction appropriate for the synthesis of Bi_2WO_6 is at 180°C. Figure 1(b) shows the XRD

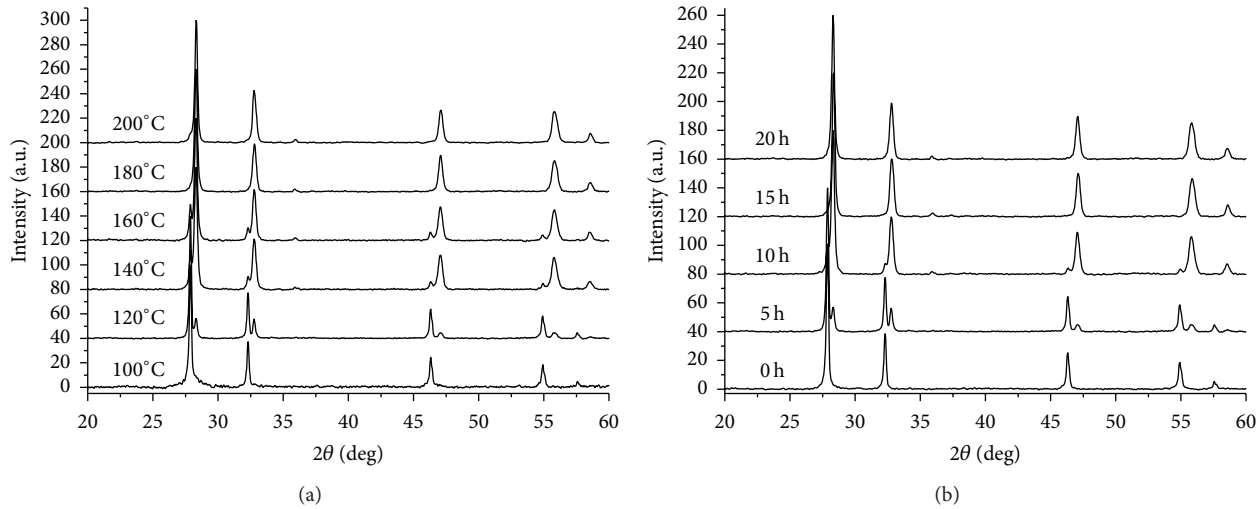

FIGURE 1: XRD patterns over the 2θ range of 20–60 deg. of the Bi_2WO_6 samples synthesized by the hydrothermal process (a) at 100–200°C for 20 h and (b) 180°C for 0–20 h.

patterns of the samples synthesized by the 180 °C and 0–20 h hydrothermal method. The cubic Bi_2O_3 phase was detected at 180°C for 0 h (before hydrothermal processing). It can be seen that the intensity of the (111) plane of cubic Bi_2O_3 phase at $2\theta = 27.93^\circ$ decreased while intensity of the (113) plane of orthorhombic Bi_2WO_6 phase at $2\theta = 28.30^\circ$ increased. It implied that the percentage of orthorhombic Bi_2WO_6 phase was increased when the reaction time was prolonged from 0 to 15 h at 180°C. When the reaction time was longer than 15 h, all the diffraction peaks can be readily indexed as a pure orthorhombic well-crystallized Bi_2WO_6 structure of the JCPDS number 73-1126 [18]. The XRD results indicate that nanosized Bi_2WO_6 could be selectively synthesized by adjusting the hydrothermal temperature and reaction time, and well-crystallized Bi_2WO_6 crystals can be synthesized at the lowest temperature of 180°C for the reaction time of longer than 15 h.

The crystal structure of Bi_2WO_6 as Aurivillius-type structure is layers of perovskite-like $(WO_4)^{2-}$ and fluorite-like $(Bi_2O_2)^{2+}$ layers lying normal to the c direction. The WO_6 octahedrons are joined by equatorial oxygen atoms, whereas the apical oxygen atoms join the WO_6 and BiO_6 polyhedrons. The tungsten exhibits a regular octahedral environment and neighbouring octahedrons are connected to each other by corner sharing. The coordination polyhedrons of bismuth are more complex but each one is bonded to six oxygen atoms [12, 19, 20]. There are only six Raman active ($2A_{1g}$ + B_{1g} + $3E_g$) and 9 IR active ($4A_{2u}$ + $5E_u$) modes for the ideal I4/mmm structure of Bi_2WO_6. These modes can be grouped into symmetric (A_{1g}) and asymmetric stretching vibrations of the WO_6 octahedrons (A_{2u} + E_u), bending vibrations of the WO_6 octahedrons (E_g + $2E_u$ + A_{2u} + B_{2u}), stretching and bending vibrations of the $(Bi_2O_2)^{2+}$ layers (B_{1g} + E_g + A_{2u}+ E_u), translational motions of the Bi^{3+} ions (A_{1g} + E_g), and vibrations involving translational motions of Bi^{3+} and W^{6+} ions (A_{2u} + E_u) [19, 20]. Raman spectra of the samples are shown in Figure 2(a). The peaks in the range 600–1000 cm^{-1} were assigned to the stretching of the W–O bonds. In more detail, the vibrations at 789.65 and 820.41 cm^{-1} of Bi_2WO_6 were associated with the antisymmetric and symmetric A_g modes of terminal O–W–O modes. The peak at 714.61 cm^{-1} was interpreted as an antisymmetric bridging mode, associated with the tungstate chains [21, 22]. The vibration of 310 cm^{-1} could be assigned to the translational mode involving simultaneous motion of Bi^{3+} and $WO_6{}^{6-}$. The peak at about 300 cm^{-1} was assigned to the mode of terminal WO_2 groups [21, 23].

Figure 2(b) shows FTIR spectra of the as-synthesized Bi_2WO_6 samples. The very weak band located at 3420 cm^{-1} can be attributed to the symmetric stretching vibration of –OH groups of adsorbed water on surface of Bi_2WO_6 samples. The spectra present the main absorption bands at 400–1000 cm^{-1} which are assigned to Bi–O stretching, W–O stretching, and W–O–W bridging stretching modes, corresponding to the Bi–O band located at 844.8 cm^{-1} and the W–O band at 821.6 cm^{-1} [24–26].

The morphologies of Bi_2WO_6 samples were revealed by field-emission scanning electron microscopy (FE-SEM) as shown in Figure 3. As seen from a low magnification FE-SEM image, the samples exhibited mainly plate-like rectangular shape with a lateral size of average length of 400–600 nm for 180°C 15 h and 300–500 nm for 180°C 20 h. Their magnified images are shown in Figures 3(b) and 3(d), which show many nanoplates with thickness of 50 nm for 180°C 15 h and 20 nm for 180°C 20 h with their smooth surfaces.

Figure 4 shows TEM images of Bi_2WO_6 samples. The as-synthesized Bi_2WO_6 at 180°C for 15 h shows uniform square nanoplates grown larger and thinner. When the reaction time was further increased to 20 h, the sample was still to be square plate-like morphology with shorter edges. The length of the edges could reach 100–150 nm. The SAED pattern confirms that the nanoplates are single crystalline Bi_2WO_6 since the

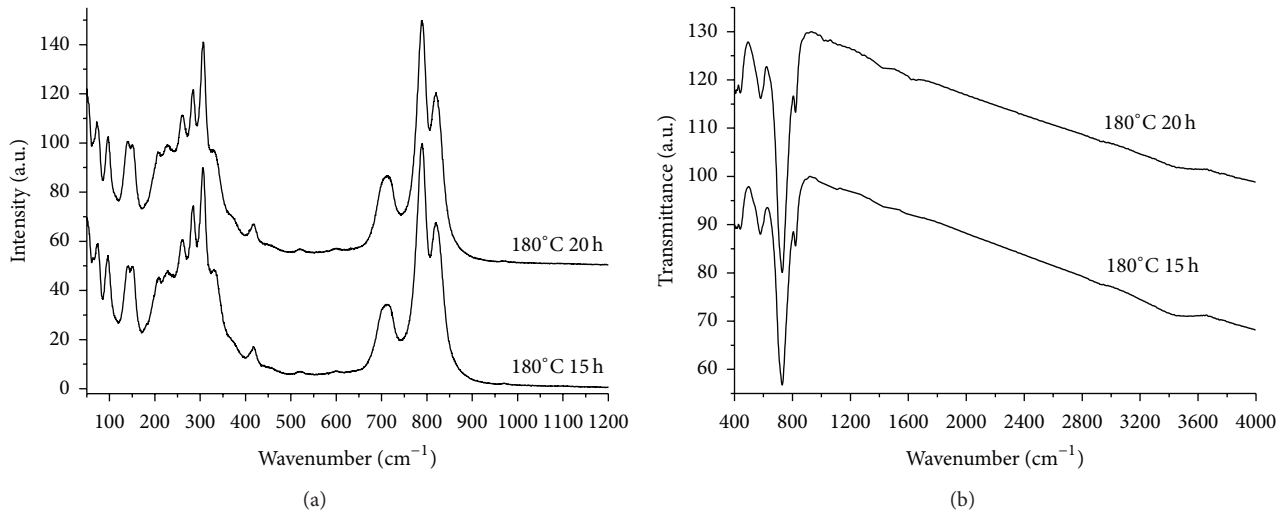

FIGURE 2: (a) Raman and (b) FTIR spectra of Bi_2WO_6 synthesized by hydrothermal process at 180°C for 15 h and 20 h.

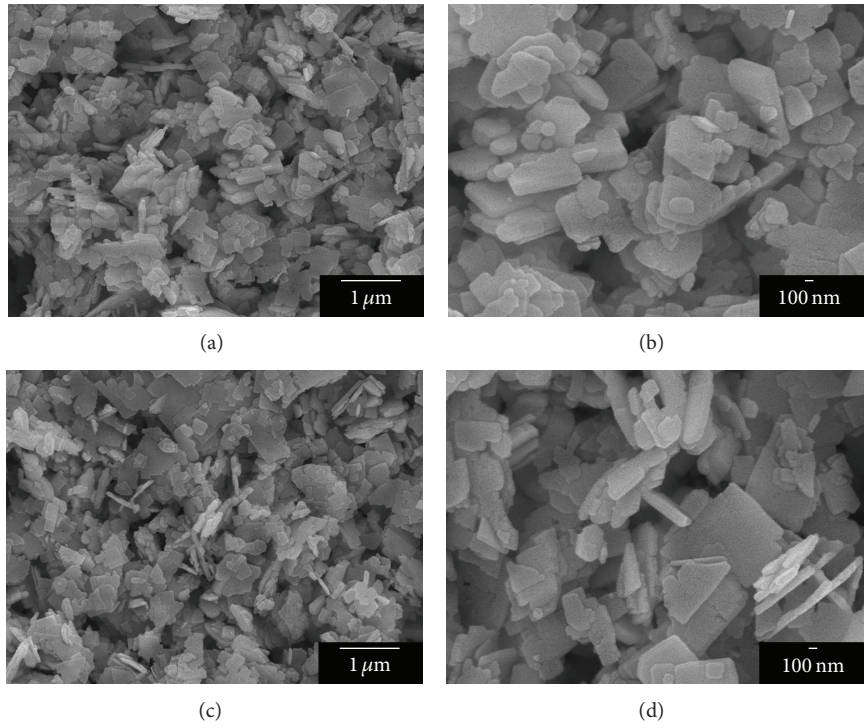

FIGURE 3: SEM images with low and high magnifications of Bi_2WO_6 synthesized by hydrothermal process at 180°C for (a, b) 15 h and (c, d) 20 h.

observed spot pattern corresponded to the most intense diffraction peaks of Bi_2WO_6. The SAED pattern reveals that the crystalline structure can be indexed to the expected orthorhombic crystal lattice of Bi_2WO_6 with characteristic (200), (220), and (020) reflection with [001] as zone axis, in agreement with the above XRD analysis. In this research, the nanoplates preferentially grew along the (001) plane, which is parallel to the $\vec{a} \times \vec{b}$ direction.

The UV-visible absorption spectrum of Bi_2WO_6 is shown in Figure 5, which shows the absorption wavelength of less than 460 nm assigned to the intrinsic energy band gap of Bi_2WO_6 [8].

To study the photocatalytic activities of the hydrothermally synthesized samples, tetraethylated rhodamine (RhB) with a major absorption band at 553 nm was chosen as a model organic pollutant. Figure 6 shows the temporal evolution of the spectra during the photodegradation of RhB photocatalyzed by typical Bi_2MoO_6 nanoplates under visible light illumination. The absorption intensity decreased gradually and the major absorption band shifted from 553 nm

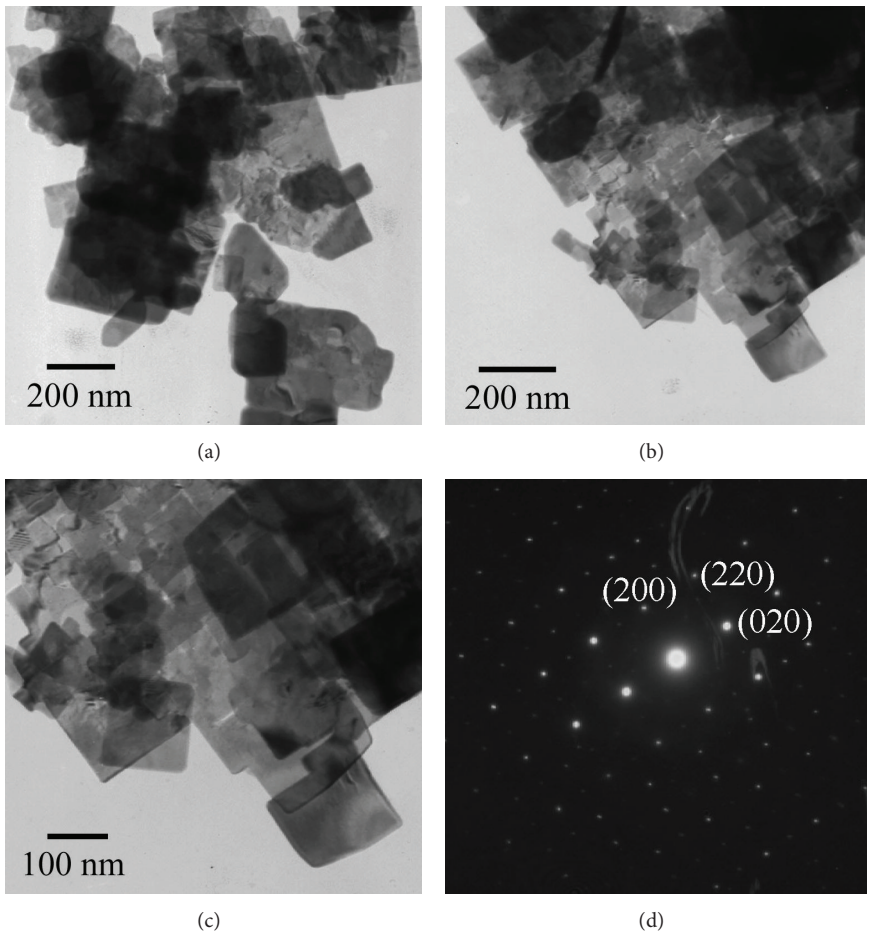

Figure 4: TEM images and SAED pattern of Bi_2WO_6 synthesized by hydrothermal process at 180°C for (a) 15 h and (b–d) 20 h.

to 498 nm in photodegradation process during 180 min, confirming that RhB (553 nm) was deethylated to rhodamine (498 nm) under visible light radiation [27, 28]. The deethylated products of RhB are N,N,N′-triethylated rhodamine (539 nm), N,N′-diethylated rhodamine (522 nm), N-ethylated rhodamine (510 nm), and rhodamine (498 nm) [29, 30]. The absorption peaks corresponding to RhB completely disappeared after about 100 min. It suggests that Bi_2WO_6 nanoplates are the excellent photocatalytic activity.

Figure 7 shows degradation efficiency of the photocatalytic Bi_2WO_6 samples against RhB. It indicates the obvious difference in percent degradation of RhB by both Bi_2WO_6 samples. The control experiment in the absence of Bi_2WO_6 catalyst under identical visible irradiation was also carried out. The results show that photodegradation of RhB by Bi_2WO_6 nanoplates synthesized at 180°C for 20 h is higher than that by Bi_2WO_6 nanoplates synthesized at 180°C for 15 h, due to its higher degree of crystallinity. In case of both Bi_2WO_6 samples, the test for the degradation of RhB was very rapid until reaching 60 min. During photocatalysis, the visible light induced photocatalytic efficiency of the Bi_2WO_6 nanoplates synthesized at 180°C for 20 h (surface area of 53.1 $m^2\ g^{-1}$) is 98.24% for RhB photodegradation. Comparing to the previous report, the photocatalytic activity of P25 TiO_2 is ~18% after 120 min under visible radiation with $\lambda > 420$ nm, reported by Cheng et al. [31]. Lu et al. [32] synthesized octahedron-like hierarchical structure of Bi_2WO_6 by a facile hydrothermal method. It shows a photodegradation of the RhB solution of 56% after the visible irradiation for 6 h. Thus, Bi_2WO_6 nanoplates show higher activities for degradation of RhB under visible light and are new candidate for visible-light-driven photocatalytic degradation of organic dyes.

The photodegradation phenomena of RhB by Bi_2WO_6 can be explained by e^-/h^+ recombination [33]. Generally, the e^-/h^+ recombination in the materials is divided into two categories: volume and surface recombination. The unique 2D layers of Bi_2WO_6 nanoplates supported the e^-/h^+ surface separation, caused by the abundant surface trapping sites and insufficient driving force for e^-/h^+ recombination. Thus, the highly photocatalytic efficiency of Bi_2WO_6 nanoplates was accelerated by the interfacial charged transfer process, which can play the role in the content and diffusion of adsorbed RhB. Their surfaces can be modified by the adsorption of some metallic atoms. In general, the e^-/h^+ recombination on the semiconductor surface is able to control with ease, because the nanosheets have large space to enhance the photochemical activity.

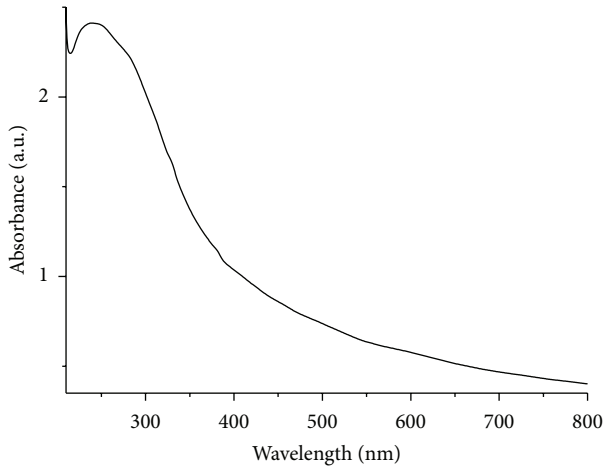

Figure 5: UV-visible absorption of Bi_2WO_6 nanoplates.

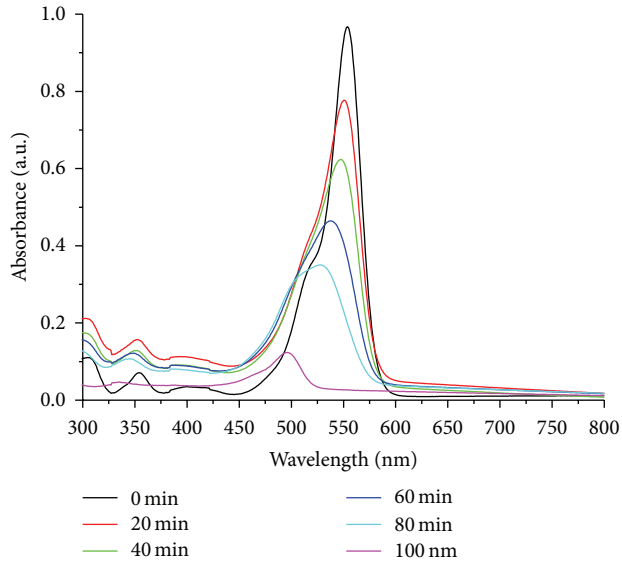

Figure 6: UV-visible absorption of RhB solution containing Bi_2WO_6 photocatalytic nanoplates synthesized by the hydrothermal process at 180°C for 20 h.

4. Conclusions

In this research, orthorhombic Bi_2WO_6 nanoplates as a photocatalyst were successfully synthesized by hydrothermal reaction at 180°C for 20 h in the solution with the pH of 10. The photocatalytic activity of Bi_2WO_6 nanoplates was determined to be 98.24% degradation of RhB for 100 min irradiated by Xe light.

Conflict of Interests

The authors declare that there is no conflict of interests regarding the publication of this paper.

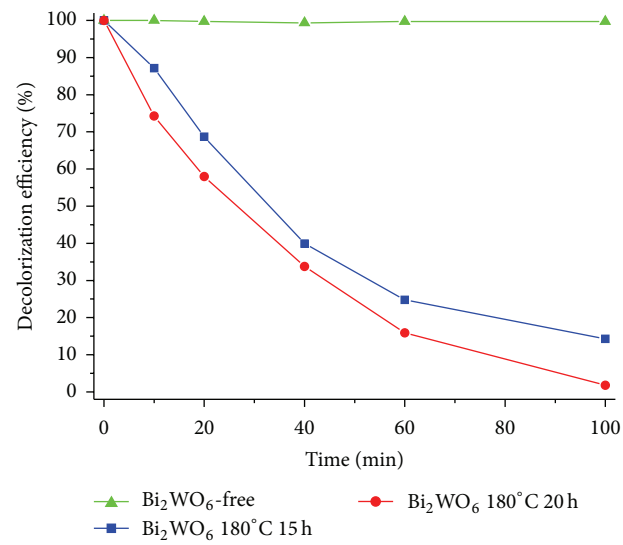

Figure 7: Decolorization efficiency of RhB solution containing Bi_2WO_6 photocatalytic nanoplates under Xe light.

Acknowledgment

The authors are extremely grateful to the Prince of Songkla University under Contact no. SCI560002S, Thailand.

References

[1] J. Xu, Y. Ao, and M. Chen, "A simple method for the preparation of Bi_2WO_6-reduced graphene oxide with enhanced photocatalytic activity under visible light irradiation," *Materials Letters*, vol. 92, pp. 126–128, 2013.

[2] J. Zhang, Z. H. Huang, Y. Xu, and F. Kang, "Sol-gel-hydrothermal synthesis of the heterostructured TiO_2/N-Bi_2WO_6 composite with high-visible-light- and ultraviolet-light-induced photocatalytic performances," *International Journal of Photoenergy*, vol. 2012, Article ID 469178, 12 pages, 2012.

[3] A. Fujishima and K. Honda, "Electrochemical photolysis of water at a semiconductor electrode," *Nature*, vol. 238, no. 5358, pp. 37–38, 1972.

[4] M. Shang, W. Wang, S. Sun, L. Zhou, and L. Zhang, "Bi_2WO_6 nanocrystals with high photocatalytic activities under visible light," *Journal of Physical Chemistry C*, vol. 112, no. 28, pp. 10407–10411, 2008.

[5] S. H. Chen, Z. Yin, S. L. Luo, X. J. Li, L. X. Yang, and F. Deng, "Photoreactive mesoporous carbon/Bi_2WO_6 composites: synthesis and reactivity," *Applied Surface Science*, vol. 259, pp. 7–12, 2012.

[6] D. O. Charkin, D. N. Lebedev, and S. M. Kazakov, "Multiple cation and anion substitutions into the structures of Bi_2WO_6 and $PbBi_3WO_8Cl$," *Journal of Alloys and Compounds*, vol. 536, pp. 155–160, 2012.

[7] M. Shang, W. Wang, and H. Xu, "New Bi_2WO_6 nanocages with high visible-light-driven photocatalytic activities prepared in refluxing EG," *Crystal Growth and Design*, vol. 9, no. 2, pp. 991–996, 2009.

[8] P. Dumrongrojthanath, T. Thongtem, A. Phuruangrat, and S. Thongtem, "Hydrothermal synthesis of Bi_2WO_6 hierarchical

flowers with their photonic and photocatalytic properties," *Superlattices and Microstructures*, vol. 54, pp. 71–77, 2013.

[9] Y. Zhuo, J. Huang, L. Cao, H. Ouyang, and J. Wu, "Photocatalytic activity of snow-like Bi_2WO_6 microcrystalline for decomposition of Rhodamine B under natural sunlight irradiation," *Materials Letters*, vol. 90, pp. 107–110, 2013.

[10] F. J. Zhang, F. Z. Xie, J. Liu, W. Zhao, and K. Zhang, "Rapid sonochemical synthesis of irregular nanolaminar-like Bi_2WO_6 as efficient visible-light-active photocatalysts," *Ultrasonics Sonochemistry*, vol. 20, pp. 209–215, 2013.

[11] Z. He, C. Sun, S. Yang, Y. Ding, H. He, and Z. Wang, "Photocatalytic degradation of rhodamine B by Bi_2WO_6 with electron accepting agent under microwave irradiation: mechanism and pathway," *Journal of Hazardous Materials*, vol. 162, no. 2-3, pp. 1477–1486, 2009.

[12] C. Belver, C. Adán, and M. Fernández-García, "Photocatalytic behaviour of Bi2MO6 polymetalates for rhodamine B degradation," *Catalysis Today*, vol. 143, no. 3-4, pp. 274–281, 2009.

[13] J. Wen, Y. Hu, K. Zhu, Y. Li, and J. Song, "High-temperature-mixing hydrothermal synthesis of ZnO nanocrystals with wide growth window," *Current Applied Physics*, vol. 14, pp. 359–365, 2014.

[14] N. Kiomarsipour and R. S. Razavi, "Hydrothermal synthesis and optical property of scale- and spindle-like ZnO," *Ceramics International*, vol. 39, pp. 813–818, 2013.

[15] Y. Fang, Z. Li, S. Xu, D. Han, and D. Lu, "Optical properties and photocatalytic activities of spherical ZnO and flower-like ZnO structures synthesized by facile hydrothermal method," *Journal of Alloys and Compounds*, vol. 575, pp. 359–363, 2013.

[16] P. V. Adhyapak, S. P. Meshram, D. P. Amalnerkar, and I. S. Mulla, "Structurally enhanced photocatalytic activity of flower-like ZnO synthesized by PEG-assited hydrothermal route," *Ceramics International*, vol. 40, pp. 1951–1959, 2014.

[17] Z. Zhang, W. Wang, M. Shang, and W. Yin, "Low-temperature combustion synthesis of Bi_2WO_6 nanoparticles as a visible-light-driven photocatalyst," *Journal of Hazardous Materials*, vol. 177, no. 1–3, pp. 1013–1018, 2010.

[18] Powder Diffract File, JCPDS-ICDD, 12 Campus Boulevard, Newtown Square, Pa, USA, (2001).

[19] M. Mączka, L. Macalik, K. Hermanowicz, L. Kępiński, and P. Tomaszewski, "Phonon properties of nanosized bismuth layered ferroelectric material—Bi_2WO_6," *Journal of Raman Spectroscopy*, vol. 41, no. 9, pp. 1059–1066, 2010.

[20] M. MacZka, J. Hanuza, W. Paraguassu, A. G. S. Filho, P. T. C. Freire, and J. M. Filho, "Phonons in ferroelectric Bi_2WO_6: raman and infrared spectra and lattice dynamics," *Applied Physics Letters*, vol. 92, no. 11, Article ID 112911, 2008.

[21] H. Fu, C. Pan, L. Zhang, and Y. Zhu, "Synthesis, characterization and photocatalytic properties of nanosized Bi_2WO_6, $PbWO_4$ and $ZnWO_4$ catalysts," *Materials Research Bulletin*, vol. 42, no. 4, pp. 696–706, 2007.

[22] R. L. Frost, L. Duong, and M. Weier, "Raman microscopy of selected tungstate minerals," *Spectrochimica Acta A*, vol. 60, no. 8-9, pp. 1853–1859, 2004.

[23] B. L. W. Zhang, Y. J. Wang, H. Y. Cheng, W. Q. Yao, and Y.-F. Zhu, "Synthesis of porous Bi_2WO_6 thin films as efficient visible-light-active photocatalysts," *Advanced Materials*, vol. 21, no. 12, pp. 1286–1290, 2009.

[24] J. Yu, J. Xiong, B. Cheng, Y. Yu, and J. Wang, "Hydrothermal preparation and visible-light photocatalytic activity of Bi_2WO_6 powders," *Journal of Solid State Chemistry*, vol. 178, no. 6, pp. 1968–1972, 2005.

[25] J. Xia, H. Li, Z. Luo et al., "Self-assembly and enhanced optical absorption of Bi_2WO_6 nests via ionic liquid-assisted hydrothermal method," *Materials Chemistry and Physics*, vol. 121, no. 1-2, pp. 6–9, 2010.

[26] G. Zhao, S. Liu, Q. Lu, and L. Song, "Controllable synthesis of Bi_2WO_6 nanofibrous mat by electrospinning and enhanced visible photocatalytic degradation performances," *Industrial & Engineering Chemistry Research*, vol. 51, pp. 10307–10312, 2012.

[27] K. Sridharan and T. J. Park, "Thorn-ball shaped TiO_2 nanostructures: Influence of Sn^{2+} doping on the morphology and enhanced visible light photocatalytic activity," *Applied Catalysis B*, vol. 134-135, pp. 174–184, 2013.

[28] L. Wu, J. Bi, Z. Li, X. Wang, and X. Fu, "Rapid preparation of Bi_2WO_6 photocatalyst with nanosheet morphology via microwave-assisted solvothermal synthesis," *Catalysis Today*, vol. 131, no. 1–4, pp. 15–20, 2008.

[29] X. Li and J. Ye, "Photocatalytic degradation of rhodamine B over $Pb_3Nb_4O_{13}$/fumed SiO_2 composite under visible light irradiation," *Journal of Physical Chemistry C*, vol. 111, no. 35, pp. 13109–13116, 2007.

[30] J. Li, H. Qiao, Y. Du et al., "Electrospinning synthesis and photocatalytic activity of mesoporous TiO_2 nanofibers," *The Scientific World Journal*, vol. 2012, Article ID 154939, 7 pages, 2012.

[31] X. Cheng, X. Yu, Z. Xing, and L. Yang, "Enhanced visible light photocatalytic activity of mesoporous anatase TiO_2 codoped with nitrogen and chlorine," *International Journal of Photoenergy*, vol. 2012, Article ID 593245, 6 pages, 2012.

[32] Y. Li, J. Liu, and X. Huang, "Synthesis and visible-light photocatalytic property of Bi_2WO_6 hierarchical octahedron-like structures," *Nanoscale Research Letters*, vol. 3, no. 10, pp. 365–371, 2008.

[33] H. Fu, L. Zhang, W. Yao, and Y. Zhu, "Photocatalytic properties of nanosized Bi_2WO_6 catalysts synthesized via a hydrothermal process," *Applied Catalysis B*, vol. 66, no. 1-2, pp. 100–110, 2006.